J. Synchrotron Rad. (1998). **5**, 667–669

Finite-element study of a toothed-crystal monochromator

J. Hrdý[a]* and J. Plešek[b]

[a]*Institute of Physics, Czech Academy of Sciences, Na Slovance 2, 18040 Praha 8, Czech Republic, and* [b]*Institute of Thermomechanics, Czech Academy of Sciences, Dolejškova 5, 18200 Praha 8, Czech Republic. E-mail: hrdy@fzu.cz*

(*Received 4 August 1997; accepted 8 December 1997*)

A toothed-crystal monochromator, proposed in previous papers, is a modification of an inclined monochromator, which reduces the impinging radiation power density on the surface of a crystal for broad synchrotron radiation beams. The surface of the monochromator has a triangular toothed structure oriented in such a way that it represents an inclined monochromator. Finite-element analysis of thermally induced deformation was performed for a particular shape of toothed crystal and for a flat crystal of the same average thickness. It was estimated that the toothed-crystal monochromator may provide 70% higher radiation power than the flat-crystal monochromator.

Keywords: X-ray monochromators; inclined monochromators.

1. Introduction

The toothed-crystal monochromator (Hrdý, 1992; Hrdý & Pacherová, 1993) is a modified version of an inclined monochromator (Hrdý, 1990, 1992; Khounsary, 1992), and has been proposed for use with broad synchrotron radiation from bending magnets and wigglers to reduce the impinging radiation power density (Fig. 1). The main advantage of the toothed geometry is that it needs a substantially smaller crystal compared with the simple inclined geometry. The simple indirectly cooled inclined monochromator has been successfully tested by the APS group (Macrander *et al.*, 1992; Lee *et al.*, 1992). Finite-element analysis of an inclined crystal monochromator has also been performed at the APS (Assoufid *et al.*, 1995; Kushnir, 1994; Rogers & Macrander, 1993).

There are basically two possible approaches to the design of a toothed-crystal monochromator. The first approach involves sufficiently large teeth which may be individually cooled (directly or indirectly, as schematically shown in Fig. 1). In this case the toothed crystal should behave like a simple inclined crystal and the only problematic part is the region around the top of the teeth. The second crystal, of course, must also be toothed to give the exit beam its original shape. For focusing of the monochromatic beam it is necessary to use a mirror.

The second approach consists of making the teeth sufficiently small (of the order of 1 mm or less) and of cooling the crystal as a whole through the base (directly or indirectly). If a fine focus is not required, then the second crystal might be flat and even sagittally bent to provide horizontal focusing. We decided to study in detail this second approach, as reported here, which also gives us an idea of what is occurring at the top of the teeth if they are individually cooled (the first approach).

2. Finite-element analysis

The shape and dimensions of the Si(111) crystal studied are shown in Fig. 2. The beam, of power density $P = 1\ \mathrm{W\ mm^{-2}}$ uniformly distributed over its cross section of 40 mm × 5 mm (both related to a plane perpendicular to the beam axis), impinges at the Bragg angle $\theta = 45^\circ$. The crystal is thermally connected through the Ga–In eutectic layer to a massive Cu plate whose temperature, $T_0 = 293$ K, is kept constant with the aid of the water-coolant system.

Finite-element analyses were performed for this toothed crystal as well as for the three flat reference Si(111) crystals with the same width and length as those of the toothed crystal and with thicknesses 0.5 mm, 1 mm and 1.5 mm. The aim of the finite-element calculations was to compare the diffraction behaviour of the toothed crystal with that of the reference crystals, namely, to compute the distortion angles (the slope errors) for all the specimens in question.

The finite-element mesh of the toothed crystal consisting of 2756 15/20 node quadratic isoparametric penta/hexahedrons (42072 DOFs) is shown in Fig. 3. Owing to symmetry, only one half of the body needed to be modelled,. Material properties of Si(111), assumed as isotropic, were chosen as $\lambda = 125\ \mathrm{W\ mK^{-1}}$, $E = 1.13 \times 10^5$ MPa, $\alpha = 2.33 \times 10^{-6}\ \mathrm{K^{-1}}$, $\nu = 0.3$, with λ being the thermal conductivity, E the Young modulus, α the thermal expansion coefficient and ν the Poisson ratio.

Since the Cu base plate had been cooled to a constant temperature T_0, the boundary conditions at the bottom surface could be written in the form

$$q = \beta(T - T_0),$$

where q is the heat flux, T is the surface temperature (yet unknown), and β is the heat transfer coefficient set as $\beta = 20\,000\ \mathrm{W\ m^{-2}\ K^{-1}}$. All the analyses were carried out as steady-state thermoelastic problems by means of the finite-element code *PMD*, version 486.3.

The results of the computation are summarized in Table 1. The first column contains the maximum vertical displacements caused by heating the crystals. The displacements were calculated at five points at the tooth face (height h is measured from the bottom surface) and at the top planes of the flat reference specimens. Similarly, the second column lists the maximum derivatives of the vertical displacements with respect to the longitudinal coordinate x, which corresponds to the maximum rotation angle (the slope

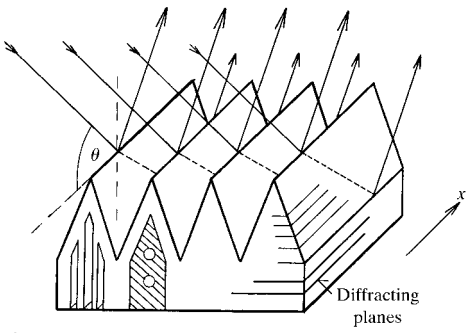

Figure 1
Schematic diagram of a toothed crystal. If the teeth are sufficiently large, they may be individually cooled, as is shown on the diagram.

Table 1
Vertical displacements and slope errors for various parts of the tooth and for the flat crystals of various thicknesses.

(*a*) Toothed crystals

h (mm)	Maximum displacement ($\times 10^{-8}$) (m)	Maximum derivative (slope error) ($\times 10^{-5}$)
1.5	1.96	0.771
1.17	1.43	0.467
0.83	1.0	0.277
0.67	0.76	0.208
0.5	0.53	0.135

(*b*) Flat crystals

Thickness (mm)	Maximum displacement ($\times 10^{-8}$) (m)	Maximum derivative (slope error) ($\times 10^{-5}$)
1.5	1.8	0.52
1.0	1.47	0.454
0.5	0.99	0.432

error) of the diffraction planes. The vertical displacement on the teeth surface as well as the slope error shows a roughly linear dependence on h.

3. Discussion of the results

It is seen from Table 1 that the tops of the teeth behave worse (the maximum displacement and its maximum derivative are larger) than the surface of any flat crystal and the lowest parts of the teeth behave better. From linear extrapolation we can estimate that the slope errors of the 0.5, 1 and 1.5 mm-thick flat crystals correspond to h = 1.11, 1.15 and 1.23 mm, respectively, measured on the toothed crystal. In other words, 39% of the toothed-crystal surface hit by radiation behaves worse (and the rest of the surface behaves better) than the 0.5 mm-thick flat crystal, 35% of the toothed-crystal surface behaves worse than the 1 mm-thick flat crystal, and 27% of the toothed-crystal surface behaves worse than the 1.5 mm-thick flat crystal. These results pertain to the power density 1 W mm^{-2}; in the following we will suppose that this percentage ratio is independent of the radiation power density (this follows from the linearity of the finite-element model).

It is known from the literature (Macrander *et al.*, 1992) that if the impinging radiation power density reaches a certain critical value, the power W_c diffracted by the double-crystal monochromator does not grow any longer and remains approximately constant. This is due to the deformations caused by increased temperature gradients. Let us suppose that the impinging power density P_c is such that the diffracted power from the double-crystal monochromator with the 1 mm-thick flat first crystal is W_c, *i.e.* reaches its saturated value. If we now replace the first flat crystal with the toothed crystal, we obtain after the second crystal

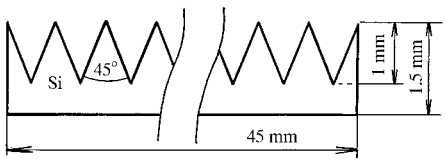

Figure 2
Dimensions of the Si(111) toothed crystal used for the finite-element analysis. The length of the crystal is 65 mm. The cross section of the X-ray beam is 40 mm × 0.5 mm, the power density is 1 W mm^{-2}, and the Bragg angle $\theta = 45°$.

the diffracted power $0.65W_c + 0.35kW_c$, where the first term corresponds to the diffraction from the part of the toothed crystal which diffracts 'better' than the flat crystal (k will be determined later). In the finite-element model the slope error increases linearly with the impinging radiation power density. Fig. 4 shows three lines: the upper line corresponds to the top of the tooth, the lowest line corresponds to the lowest part of the tooth and the dashed line corresponds to that part of tooth (h = 1.15 mm) which has the same slope error as the 1 mm-thick flat crystal. The line slopes are determined from Table 1 as the ratio of the maximum derivative (slope error) to the impinging power density 1 W mm^{-2}. The horizontal line represents the critical slope error which causes the saturation of diffracted power. It is seen from this graph that at $0.6P_c$ the diffraction from the top of the tooth becomes saturated, at P_c the diffraction from the part of the tooth at h = 1.15 mm as well as from the surface of the 1 mm-thick flat crystal becomes saturated and, finally, at $3.36P_c$ the diffraction from the lowest part of the tooth becomes saturated. Then the contribution of the upper part of the tooth (above h = 1.15 mm) to the total saturated power is $[0.35(0.6 + 1)/2]W_c$ and the contribution of the lower part of the tooth is $[0.65(1 + 3.36)/2]W_c$.

The saturated diffracted power from the whole toothed monochromator is then $1.7W_c$, *i.e.* 70% higher compared with the flat crystal of the same average thickness. (In the same way it may be shown that the saturated diffracter power from the toothed crystal is 28% higher than that from the 0.5 mm-thick flat crystal.)

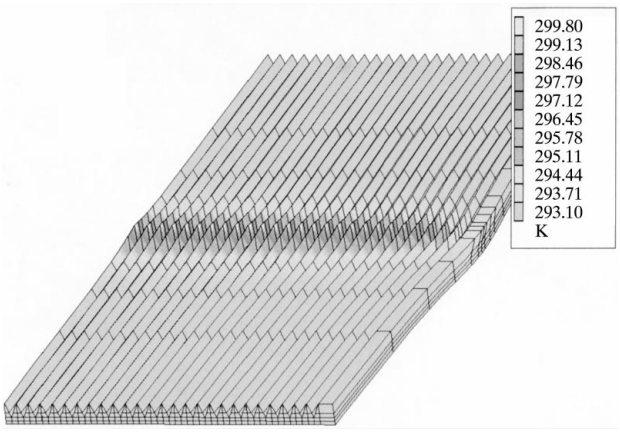

Figure 3
Deformed shape of the finite-element mesh and flat contours showing the temperature field.

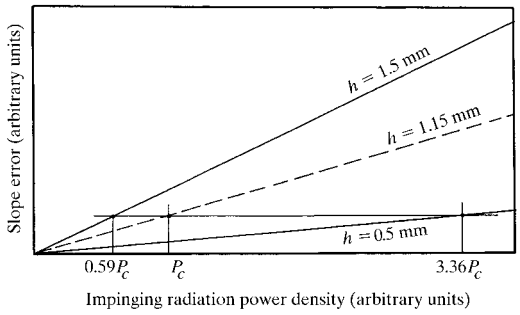

Figure 4
Slope errors as functions of impinging radiation power density for three different points situated at the tooth surface.

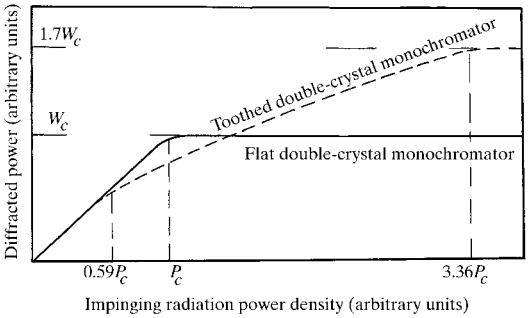

Figure 5
Schematic diagram of the expected behaviour of toothed and 1 mm-thick flat double-crystal monochromators.

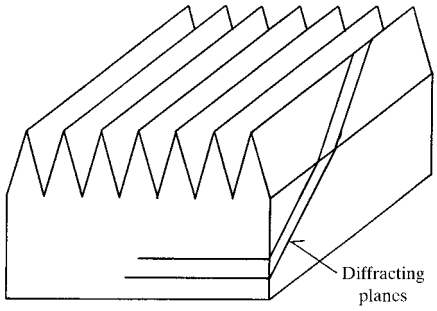

Figure 6
The teeth may be produced in the asymmetrically cut crystal to combine the inclined and asymmetric diffraction in order to decrease the impinging radiation power density.

During the increase of the impinging power density, the expected behaviour of toothed and flat crystals is as follows (Fig. 5). Below $0.6P_c$ the behaviour of both crystals is similar. Then the diffracted power from the toothed monochromator increases more slowly than the diffracted power from the flat-crystal monochromator (due to the 'worse' behaviour of the upper part of the teeth). Above P_c the diffracted power from the flat-crystal monochromator is saturated (W_c) whereas the diffracted power from the toothed monochromator increases until it reaches the saturated value $1.7W_c$.

The consequence of the above model is that the local diffracted intensity and the percentage of harmonics contamination will vary horizontally across the teeth profile in the saturation regime due to the heat load. This may complicate some experiments in the case of absence of subsequent sagittal focusing.

The finite-element analysis also revealed a small convex sagittal bending of diffracting planes in the toothed crystal. This creates an angular deviation, ξ, of the diffracting planes from the original 'cool' planes position on the surface of the teeth. This deviation ξ is zero on the top and on the lowest part of the teeth and reaches its maximum value near $h = 1$ mm. The estimated value of ξ for $h = 1$ mm is approximately 3×10^{-6}. As the consequent changes of the Bragg angles on both crystals are of the order of ξ^2 (for θ far from 90°), the sagittal bending will not influence the diffracted power. It may, however, contribute to the focusing effect described by Hrdý *et al.* (1997).

The above consideration is undoubtedly very schematic and requires more theoretical and experimental work. In order for the toothed monochromator to be more efficient under high heat loads than the flat-crystal monochromator, it is necessary that the vertical dimension of the beam be smaller than the size of the teeth. In this case the radiation footprint on the first crystal has a typical zigzag shape and the heat has enough space to flow to the sides. If the vertical size of the beam was much larger than the size of the teeth, then the footprint is basically the same as in the case of the flat crystal and the toothed geometry would not be an improvement.

The above toothed crystal is based on the toothed structure fabricated into a symmetrically diffracting crystal (diffracting planes are parallel with the surface). Its function may be improved by fabricating the teeth into an asymmetrically diffracting crystal to combine the inclined and asymmetric diffraction (Fig. 6). This represents the modification of a general asymmetric (Smither & Fernandez, 1994) or rotated-inclined (Kamiya *et al.*, 1995) monochromator so that they may be used for broad beams from bending magnets or wigglers.

This work was partially supported by the Commission of the European Communities, contract No. IC15-CT96-0753 (DG 12-SNRD), the Grant Agency of the Czech Republic, contract No. 101/96/0910, and the MPO, Czech Republic, contract No. PZ-CH/22/97.

References

Assoufid, L., Lee, W. K. & Mills, D. M. (1995). *Rev. Sci. Instrum.* **66**(3), 2713–2718.
Hrdý, J. (1990). Technical Note ST/S-TN-90/27. Sincrotrone Trieste, Trieste, Italy.
Hrdý, J. (1992). *Rev. Sci. Instrum.* **63**, 459–460.
Hrdý, J. & Pacherová, O. (1993). *Nucl. Instrum. Methods*, A**327**, 605–611.
Hrdý, J., Pascarelli, S., D'Acapito, F., Colonna, S. & Mobilio, S. (1997). *J. Synchrotron Rad.* **5**, 54–56.
Kamiya, N., Uruga, T., Kimura H., Yamaoka, H., Yamamoto, M., Kawano, Y., Ishikawa, T., Kitamura, H., Ueki, T., Iwasaki, H., Kashihara, Y., Tanaka, N., Moriyama, H., Hamada, K., Miki, K. & Tanaka, I. (1995). *Rev. Sci. Instrum.* **66**(2), 1703–1705.
Khounsary, A. M. (1992). *Rev. Sci. Instrum.* **63**, 461–464.
Kushnir, V. (1994). *Rev. Sci. Instrum.* **65**(11), 3403–3407.
Lee, W. K., Macrander, A. T., Mills, D. M., Rogers, C. S., Smither, R. K. & Berman, L. E. (1992). *Nucl. Instrum. Methods*, A**320**, 381–387.
Macrander, A. T., Lee, W. K., Smither, R. K., Mills, D. M., Rogers, C. S. & Khounsary, A. M. (1992). *Nucl. Instrum. Methods*, A**319**, 188–196.
Rogers, C. S. & Macrander, A. T. (1993). *Nucl. Instrum. Methods*, A**335**, 561–568.
Smither, R. K. & Fernandez, P. B. (1994). *Nucl. Instrum. Methods*, A**347**, 313–319.